Research Article | Vol. 32, No. 6 / 11 Mar 2024 / Optics Express 10690
Optics EXPRESS

Scattering of partially coherent electromagnetic beams by a sphere

HUGO F. SCHOUTEN[1,2] AND TACO D. VISSER[1,2,*]

[1]School of Physics and Electronics, Shandong Normal University, Jinan, China
[2]Dept. of Physics and Astronomy, Vrije Universiteit, Amsterdam, The Netherlands
[*]t.d.visser@vu.nl

Abstract: We examine the scattering of a partially coherent, partially polarized electromagnetic beam by a homogeneous sphere (Mie scattering). The degree of polarization and the Stokes parameters in the far zone are found to be strongly dependent on the state of coherence and polarization of the incident beam. In particular, we demonstrate the emergence of polarization singularities and show that partial spatial coherence gives rise to significant depolarization effects. In addition we explore the symmetry properties of the scattered field.

1. Introduction

The role of spatial coherence in optical processes is quite profound. It influences a beam's propagation, directionality, and interaction with material media [1,2]. For the case of scattering by a homogeneous sphere, so-called Mie scattering [3,4], significant coherence effects are known to occur when the incident field's transverse coherence length is comparable to the sphere radius [5–11]. The analysis of spatial coherence in scattering is typically limited to scalar fields, two exceptions being [12], which focuses on the intensity of the scattered field, and [13]. In the latter, a Muller matrix formalism was developed which was successfully compared with numerical results of the discrete dipole approximation. The theory was also applied to large water droplets and hexagonal ice crystals. Corona, glory and halo effects were found to disappear for highly incoherent incident light.

In the present study the state of polarization of the far-zone scattered field is examined. Our approach is inspired by the works of Lahiri and Wolf [14,15] on reflection and refraction of random beams at a planar interface. As we will show, Mie scattering is strongly influenced by the spatial coherence and the degree of polarization (DoP) of the incoming radiation. For example, if the incident beam is partially coherent and linearly polarized, say along the x-direction, then the scattered field can acquire a y-component. For a fully coherent beam such a depolarization does not occur. Another result is that for partially coherent, linearly polarized light, the scattered field in certain directions can be completely unpolarized. A slight perturbation changes these zeros of the DoP into polarization singularities (C-points). Furthermore, we show how spatial coherence affects the symmetry properties of the Stokes parameters of the the scattered field.

For sunlight in the visible range the transverse coherence length is around 50 μm [16], which is comparable to the size of many aerosoles. Both the depolarization and the modified intensity distribution caused by partial coherence also play a role in multiple scattering, meaning that the radiative transport process [17] will also be affected. The effects that we describe are therefore expected to play an important role in atmospheric processes that determine weather and climate. Similarly, when in remote sensing a fully coherent laser source is used, propagation through atmospheric turbulence will render the beam partially coherent and partially polarized. Thus, in that case too, Mie scattering will be altered.

#518782 https://doi.org/10.1364/OE.518782
Journal © 2024 Received 12 Jan 2024; revised 21 Feb 2024; accepted 21 Feb 2024; published 8 Mar 2024

Optics EXPRESS

2. Partially coherent electromagnetic beams

We consider the scattering of a spatially partially coherent, partially polarized electromagnetic beam by a homogeneous dielectric sphere, as sketched in Fig. 1. The sphere, with radius a and refractive index n, is centered at the origin O of a Cartesian coordinate system. The incident beam propagates along the positive z-direction and is characterized, at frequency ω, by a cross-spectral density (CSD) matrix of the form [2, Ch. 9]

$$W_{ij}^{(\mathrm{inc})}(\rho_{01}, \rho_{02}; \omega) = \langle E_i^{(\mathrm{inc})*}(\rho_{01}; \omega) E_j^{(\mathrm{inc})}(\rho_{02}; \omega) \rangle, \quad i, j \in \{x_0, y_0\}. \tag{1}$$

Here $\rho_0 = (x_0, y_0)$ indicates a position in the plane transverse to the beam axis, $E_i^{(inc)}$ is a Cartesian component of the electric field, and the angular brackets indicate ensemble averaging. We emphasize that the beam does not need not be rotationally symmetric. For brevity, we henceforth no longer display the frequency dependence of the various quantities.

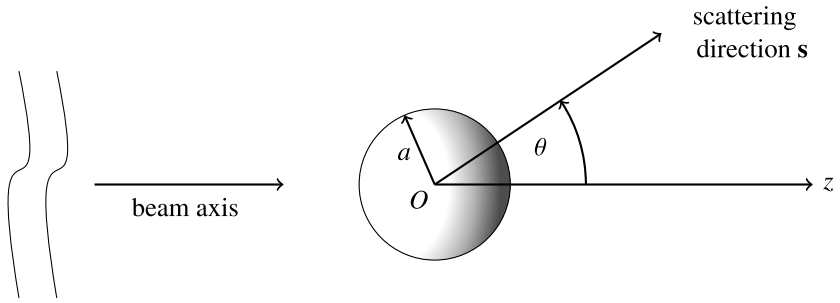

Fig. 1. Geometry of scattering of a spatially partially coherent, partially polarized beam by a homogeneous sphere.

The incident beam is assumed to be of the Gaussian Schell-model (GSM) type, with an effective width much larger than the particle radius. In that case, for $z_1 = z_2 = 0$, its CSD matrix can be written as [2]

$$W_{ij}^{(\mathrm{inc})}(\rho_{01}, \rho_{02}) = A_i A_j B_{ij} \mathrm{e}^{-(\rho_{02} - \rho_{01})^2/(2\delta_{ij}^2)}. \tag{2}$$

Here A_i is the amplitude of the Cartesian field components, B_{ij} represents their correlation, and the four coherence radii are denoted δ_{ij}. These parameters are defined with respect to the (x_0, y_0) system. several constraints [2,18] that are listed in the Supplement 1. The spectral Stokes parameters [2] for this beam are readily found to be

$$\begin{aligned} S_0 &= A_x^2 + A_y^2, \\ S_1 &= A_x^2 - A_y^2, \\ S_2 &= 2A_x A_y \,\mathrm{Re}\left(B_{xy}\right), \\ S_3 &= 2A_x A_y \,\mathrm{Im}\left(B_{xy}\right). \end{aligned} \tag{3}$$

The direction of observation $\mathbf{s}$ has coordinates $\mathbf{s} = (\cos\phi \sin\theta, \sin\phi \sin\theta, \cos\theta)^{\mathrm{T}}$, with ϕ and θ spherical angles. It will be convenient to take this direction to be in the xz-plane. This is achieved by a coordinate rotation over an angle ϕ around the z-axis, such that $(x_0, y_0) \rightarrow (x, y)$, as illustrated in Fig. 2. The rotation changes the elements of the CSD matrix into [1, p. 347]

$$W_{\alpha\beta}^{(\mathrm{inc})}(\rho_1, \rho_2) = \sum_{i,j} U_{\alpha i} U_{\beta j} W_{ij}^{(\mathrm{inc})}(\rho_{01}, \rho_{02}), \quad \alpha, \beta \in \{x, y\}, \tag{4}$$

Optics EXPRESS

where $\rho = (x, y)$ and

$$\mathbf{U} = \begin{pmatrix} \cos\phi & \sin\phi \\ -\sin\phi & \cos\phi \end{pmatrix}. \tag{5}$$

Thus, after this rotation, the CSD elements are

$$W^{(inc)}_{\alpha\beta}(\rho_1, \rho_2) = \sum_{i,j} U_{\alpha i} U_{\beta j} A_i A_j B_{ij} \mathrm{e}^{-(\rho_2-\rho_1)^2/(2\delta_{ij}^2)}, \quad i, j \in \{x_0, y_0\} \tag{6}$$

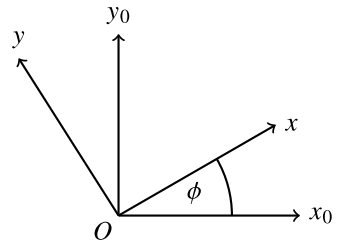

Fig. 2. Rotation of the original coordinate system, (x_0, y_0, z), over an angle ϕ around the z-axis to the system (x, y, z). The direction of observation $\mathbf{s}$ has no component along the y-axis.

In the partially coherent case, the electric field vector of the incident beam can be expressed as an angular spectrum of plane waves propagating in a range of directions $\mathbf{u}$ [1, Sec. 3.2], i.e.,

$$\mathbf{E}^{(\mathrm{inc})}(\mathbf{r}) = \iint_{|\mathbf{u}_\perp|\le 1} \mathbf{D}(u_x, u_y) \mathrm{e}^{\mathrm{i}k\mathbf{u}\cdot\mathbf{r}} \, \mathrm{d}^2 u_\perp, \tag{7}$$

with $\mathbf{r} = (x, y, z)^{\mathrm{T}}$, k the free-space wavenumber corresponding to frequency ω, and

$$\mathbf{E}^{(\mathrm{inc})}(\mathbf{r}) = \begin{pmatrix} E_x \\ E_y \end{pmatrix} \quad \text{and} \quad \mathbf{D}(u_x, u_y) = \begin{pmatrix} D_x \\ D_y \end{pmatrix}, \tag{8}$$

where $\mathbf{D}$ is the vectorial amplitude of the wave propagating in the direction $\mathbf{u}$. Furthermore, we introduce the notation

$$\mathbf{u} = (u_x, u_y, u_z)^{\mathrm{T}}, \quad \mathbf{u}_\perp = (u_x, u_y)^{\mathrm{T}}, \tag{9}$$

with

$$u_z = \sqrt{1 - u_x^2 - u_y^2}. \tag{10}$$

The last expression, together with the domain of integration in Eq. (7), implies that evanescent waves are not taken into account. On using Eq. (7) in the definition (1) in the rotated system, we obtain

$$W^{(\mathrm{inc})}_{\alpha\beta}(\rho_1, \rho_2) = \iint_{\mathcal{V}} \mathcal{A}_{\alpha\beta}(\mathbf{u}'_\perp, \mathbf{u}''_\perp) \mathrm{e}^{ik(\mathbf{u}''_\perp\cdot\rho_2 - \mathbf{u}'_\perp\cdot\rho_1)} \, d^2u'_\perp d^2u''_\perp \tag{11}$$

where $\mathcal{V} = \{(\mathbf{u}'_\perp, \mathbf{u}''_\perp) \in \mathbb{R}^2 \times \mathbb{R}^2 | \, |\mathbf{u}'_\perp| \le 1 \wedge |\mathbf{u}''_\perp| \le 1\}$, and with the angular correlation matrix defined as [1, Sec. 5.6.3]

$$\mathcal{A}_{\alpha\beta}(\mathbf{u}'_\perp, \mathbf{u}''_\perp) = \langle D^*_\alpha(\mathbf{u}'_\perp) D_\beta(\mathbf{u}''_\perp) \rangle. \tag{12}$$

This matrix can be expressed as a 4D-Fourier transform of the CSD matrix, namely [1, Eq. (5.6–49)]

$$\mathcal{A}_{\alpha\beta}(\mathbf{u}'_\perp, \mathbf{u}''_\perp) = k^4 \tilde{W}^{(inc)}_{\alpha\beta}(-k\mathbf{u}'_\perp, k\mathbf{u}''_\perp), \tag{13}$$

Optics EXPRESS

where

$$\tilde{W}^{(\mathrm{inc})}_{\alpha\beta}(\mathbf{f}_1,\mathbf{f}_2)=\frac{1}{(2\pi)^4}\iint_{-\infty}^{\infty}W^{(\mathrm{inc})}_{\alpha\beta}(\rho_1,\rho_2)\mathrm{e}^{-i(\mathbf{f}_1\cdot\rho_1+\mathbf{f}_2\cdot\rho_2)}\,\mathrm{d}^2\rho_1 d^2\rho_2. \tag{14}$$

From Eq. (6) it follows that

$$\begin{aligned}\tilde{W}^{(\mathrm{inc})}_{\alpha\beta}(-k\mathbf{u}'_\perp,k\mathbf{u}''_\perp)=\sum_{i,j}U_{\alpha i}U_{\beta j}\frac{A_iA_jB_{ij}\delta_{ij}^2}{2\pi}\delta^2\left[k\left(\mathbf{u}''_\perp-\mathbf{u}'_\perp\right)\right]\\ \times\exp\left[-\frac{1}{8}\delta_{ij}^2k^2(\mathbf{u}''_\perp+\mathbf{u}'_\perp)^2\right].\end{aligned} \tag{15}$$

We next turn our attention to the far-zone scattered field, $\mathbf{E}^{(\mathrm{sca})}(\mathbf{r})=(E^{(\mathrm{sca})}_\theta,E^{(\mathrm{sca})}_\phi)^{\mathrm{T}}$, with both components orthogonal to the scattering direction $\mathbf{s}=\mathbf{r}/|r|$. For a single incident plane wave, with amplitudes D_x and D_y and propagation direction $\mathbf{u}_0$, the scattered field is of the form

$$\mathbf{E}^{(\mathrm{sca})}(r\mathbf{s})=\mathbf{f}(\mathbf{s},\mathbf{u}_0)\begin{pmatrix}D_x(\mathbf{u}_0)\\D_y(\mathbf{u}_0)\end{pmatrix}\frac{e^{\mathrm{i}kr}}{r}, \tag{16}$$

with $\mathbf{f}$ the 2×2 scattering amplitude matrix

$$\mathbf{f}(\mathbf{s},\mathbf{u}_0)=\begin{pmatrix}f_{\theta x}&f_{\theta y}\\f_{\phi x}&f_{\phi y}\end{pmatrix}, \tag{17}$$

with arguments

$$\mathbf{s}=(\sin\theta,0,\cos\theta)^{\mathrm{T}}, \tag{18}$$

$$\mathbf{u}_0=(u_{0x},u_{0y},u_{0z})^{\mathrm{T}}. \tag{19}$$

Its precise derivation, which, following Lahiri and Wolf [14], involves several successive coordinate transformations is presented in the Supplement 1. Note that having $s_y=0$ in Eq. (18) is a consequence of the rotation shown in Fig. 2. On using the angular spectrum expression (7), we can thus write

$$E^{(\mathrm{sca})}_p(r\mathbf{s})=\frac{e^{ikr}}{r}\int_{|\mathbf{u}'_\perp|\le1}\sum_{m=x,y}f_{pm}(\mathbf{s},\mathbf{u}')D_m(\mathbf{u}'_\perp)\,\mathrm{d}^2u'_\perp,\quad p\in\{\theta,\phi\}. \tag{20}$$

In contrast to the fully coherent case, the matrix $\mathbf{f}$ is found to be no longer diagonal. This means that an incident beam that is, say, x-polarized may generate a scattered field with a non-zero y-component. In other words, partial coherence can cause depolarization. We will encounter some striking examples of this phenomenon in the next section.

Since we are interested in one-point quantities, namely the degree of polarization (DoP) and the Stokes parameters, we need to only consider matrix elements at two coincident points. Using Eqs. (12) and (20), these can be written as

$$W^{(\mathrm{sca})}_{pq}(r\mathbf{s},r\mathbf{s})\equiv\langle E^{(\mathrm{sca})*}_p(r\mathbf{s})E^{(\mathrm{sca})}_q(r\mathbf{s})\rangle,\quad p,q\in\{\theta,\phi\} \tag{21}$$

$$=\frac{1}{r^2}\sum_{m,n}\iint_{\mathcal{V}}f^*_{pm}(\mathbf{s},\mathbf{u}')f_{qn}(\mathbf{s},\mathbf{u}'')\mathcal{A}_{mn}(\mathbf{u}'_\perp,\mathbf{u}''_\perp)\,\mathrm{d}^2u''_\perp\mathrm{d}^2u_\perp. \tag{22}$$

On substituting from Eqs. (13) and (15) we thus obtain

$$\begin{aligned}W^{(\mathrm{sca})}_{pq}(r\mathbf{s},r\mathbf{s})=\frac{1}{r^2}\sum_{i,j,m,n}U_{mi}U_{nj}\frac{A_iA_jB_{ij}\delta_{ij}^2}{2\pi k^2}\int_{|\mathbf{u}'_\perp|\le1}e^{-\delta_{ij}^2k^2u'^2_\perp/2}\\ \times f^*_{pm}(\mathbf{s},\mathbf{u}')f_{qn}(\mathbf{s},\mathbf{u}')\,\mathrm{d}^2u'_\perp.\end{aligned} \tag{23}$$

Optics EXPRESS

This expression, from which all relevant quantities can be derived, is evaluated numerically in the examples presented in the next section. Note that in [13] a similar formalism is used to derive Muller matrix elements.

The far-zone spectral Stokes parameters are defined as [2]

$$S_0(r\mathbf{s}) = W^{(\mathrm{sca})}_{\theta\theta}(r\mathbf{s}, r\mathbf{s}) + W^{(\mathrm{sca})}_{\phi\phi}(r\mathbf{s}, r\mathbf{s}), \tag{24}$$

$$S_1(r\mathbf{s}) = W^{(\mathrm{sca})}_{\theta\theta}(r\mathbf{s}, r\mathbf{s}) - W^{(\mathrm{sca})}_{\phi\phi}(r\mathbf{s}, r\mathbf{s}), \tag{25}$$

$$S_2(r\mathbf{s}) = W^{(\mathrm{sca})}_{\theta\phi}(r\mathbf{s}, r\mathbf{s}) + W^{(\mathrm{sca})}_{\phi\theta}(r\mathbf{s}, r\mathbf{s}), \tag{26}$$

$$S_3(r\mathbf{s}) = \mathrm{i}\left[W^{(\mathrm{sca})}_{\phi\theta}(r\mathbf{s}, r\mathbf{s}) - W^{(\mathrm{sca})}_{\theta\phi}(r\mathbf{s}, r\mathbf{s})\right]. \tag{27}$$

Expressing these parameters in terms of θ and ϕ reduces to the usual x and y expressions when scattering along the z-axis is considered. From the Stokes parameters the DoP, denoted $\mathcal{P}$, as well as ψ, the angle of the major axis of the polarization ellipse associated with the polarized portion of the field, can both be readily found through the expressions [19]

$$\mathcal{P} = \frac{\sqrt{S_1^2 + S_2^2 + S_3^2}}{S_0}, \tag{28}$$

and

$$\tan(2\psi) = \frac{S_2}{S_1}. \tag{29}$$

For the incident beam given by Eq. (3) this means that

$$\tan(2\psi_0) = \frac{2A_xA_y\,\mathrm{Re}(B_{xy})}{A_x^2 - A_y^2}. \tag{30}$$

3. Numerical results

There is a total of five observable quantities to consider, namely the spectral density ("intensity at a single frequency"), the degree of polarization, and the Stokes parameters S_1, S_2 and S_3. These all depend on the angles θ and ϕ, and nine parameters (n, a, A_x, A_y, $\mathrm{Re}(B_{xy})$, $\mathrm{Im}(B_{xy})$, and the three δ_{ij}). Clearly then, we must limit ourselves in presenting our results. In all examples we set $n = 1.33$, $A_x = A_y$, and $a = 5\lambda$. That means that the dependence of the far-zone quantities, as well as their symmetry properties, are examined as functions of B_{xy} and the coherence radii δ_{ij}.

Partial linear polarization

Figure 3 shows a color-coded representation of the spectral density as observed from infinity. Different points represent different far-zone viewing angles (and are not to be confused with the actual spherical scatterer). The arrow indicates the beam axis (the positive z-axis) and the solid black circle specifies the xz-plane. The dashed circle shows the major axis of the polarization ellipse of the polarized portion of the incident field [Eq. (30)]. The correlation coefficient B_{xy} is taken to be real-valued. It is seen from Eq. (3) that the incident beam is then partially linearly polarized. Also, since $A_x = A_y$, $|B_{xy}|$ is equal to $\mathcal{P}^{(\mathrm{inc})}$, the DoP of the incident field. Furthermore, the three coherence radii are all chosen to be equal to the sphere radius, i.e., $\delta_{xx} = \delta_{yy} = \delta_{xy} = a = 5\lambda$. Clearly visible, in Fig. 3(a), is the relatively high scattered intensity in the forward direction. In Fig. 3(b) the back-scattered field can be seen. The results for the θ-dependence of the intensity are in line with those reported in [6] and [13], where the results of the partially coherent case are compared with the (nearly) coherent one. Although the variation along the axial ϕ direction is seen to be weak in both figures, the mirror symmetry with respect

Optics EXPRESS

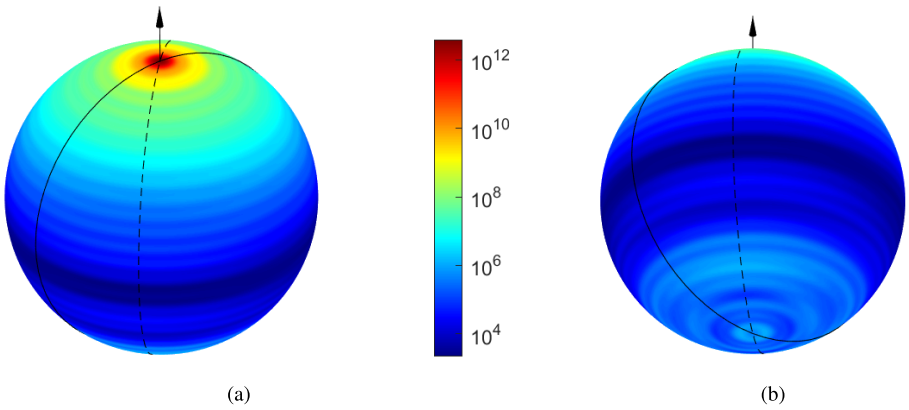

Fig. 3. Far-zone spectral density [a.u.] for a partially coherent, partially linearly polarized beam scattered by a sphere from two different perspectives. In this example $B_{xy} = 0.5$, $\delta_{xx} = \delta_{yy} = \delta_{xy} = 5\,\lambda$.

to the incident polarization direction (dashed curve) is visible in Fig. 3(b). Visualization 1 shows a continuous range of viewing angles.

The degree of polarization of the scattered field, denoted $\mathcal{P}^{(\mathrm{sca})}$, as a function of the (real) correlation coefficient B_{xy} is shown in Figs. 4–6. For a completely unpolarized incident beam ($B_{xy} = 0$), the rotationally symmetric scattered field can have a DoP as high as 0.7 (see Fig. 4). As expected, in most directions $\mathcal{P}^{(\mathrm{sca})}$ increases with increasing B_{xy}. This is shown in Fig. 5 for $B_{xy} = 0.5$. In some directions the scattered field is seen to be almost fully polarized, with $\mathcal{P}^{(\mathrm{sca})} = 0.9$. In other directions, as will be shown later, the $\mathcal{P}^{(\mathrm{sca})}$ can be exactly zero. If the incident beam is fully polarized ($B_{xy} = 1$), the scattered field is highly polarized in most directions, however, in other directions the DoP is as low as 0.02 (near $\theta = 180°$), as shown in Fig. 6. This absence of complete polarization in all directions is a consequence of partial coherence. The results for the full range of B_{xy} values is shown in the left-hand panel of Visualization 2.

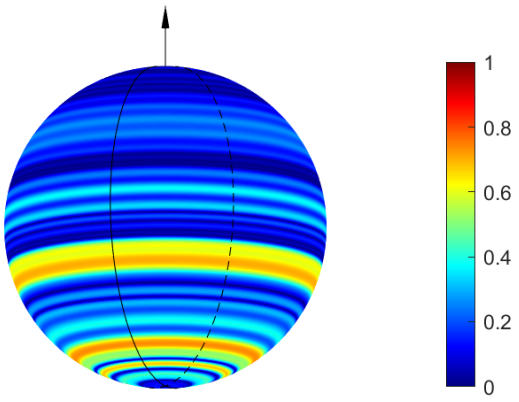

Fig. 4. The degree of polarization $\mathcal{P}^{(\mathrm{sca})}$ when the correlation coefficient of the incident field $B_{xy} = 0$. Note that in this case $\mathcal{P}^{(\mathrm{in})} = B_{xy} = 0$. Also, $\delta_{xx} = \delta_{yy} = \delta_{xy} = a = 5\,\lambda$.

Optics EXPRESS

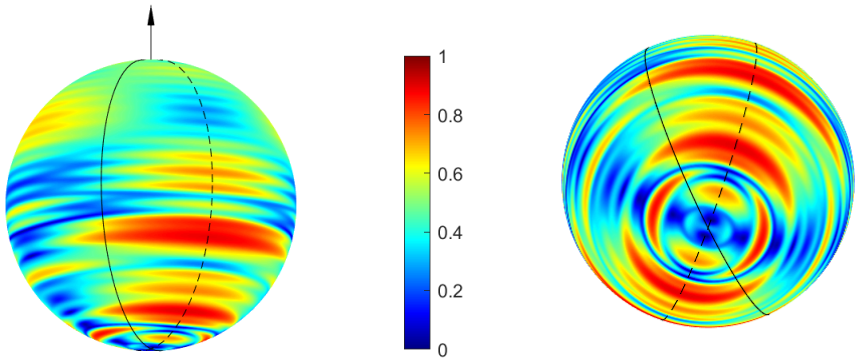

(a) (b)

Fig. 5. Two perspectives of the degree of polarization $\mathcal{P}^{(\mathrm{sca})}$ when the correlation coefficient of the incident field $B_{xy} = \mathcal{P}^{(\mathrm{in})} = 0.5$. All other parameters are as in Fig. 4.

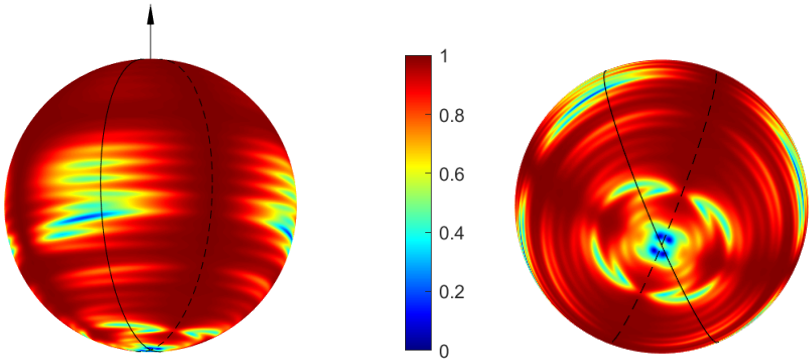

(a) (b)

Fig. 6. Two perspectives of the degree of polarization $\mathcal{P}^{(\mathrm{sca})}$ when the incident beam is fully polarized, i.e., $B_{xy} = \mathcal{P}^{(\mathrm{in})} = 1$. All other parameters are as in Fig. 4.

Optics EXPRESS

Symmetries

The scattered field has certain symmetry properties. First, for the incident field given by Eq. (2) one has

$$W_{ij}^{(\mathrm{inc})}(\rho_{01},\rho_{02}) = W_{ij}^{(\mathrm{inc})}(-\rho_{01},-\rho_{02}), \quad i,j \in \{x,y\}. \tag{31}$$

which implies a point symmetry for the matrix elements of the scattered field, i.e.,

$$W_{pq}^{(\mathrm{sca})}(\theta,\phi) = W_{pq}^{(\mathrm{sca})}(\theta,\phi+180^\circ), \quad p,q \in \{\theta,\phi\}. \tag{32}$$

This can verified by considering the behavior of the matrices $\mathbf{U}$ in Eq. (23). Clearly, all one-point quantities in the far zone, such as the Stokes parameters, share this point symmetry. Second, the orientation angle ψ_0 of the linearly polarized part of the incident beam [see Eq. (30)] determines several mirror symmetries. These turn out to be

$$W_{pp}^{(\mathrm{sca})}(\theta,\psi_0+\Delta\phi) = W_{pp}^{(\mathrm{sca})}(\theta,\psi_0-\Delta\phi), \tag{33}$$

$$W_{pq}^{(\mathrm{sca})}(\theta,\psi_0+\Delta\phi) = -W_{pq}^{(\mathrm{sca})}(\theta,\psi_0-\Delta\phi) \quad p\neq q, \tag{34}$$

for any value of $\Delta\phi$.

Combining the point symmetry expressed by Eq. (32) with the above (anti-)mirror symmetry with respect to the angle ψ_0 implies yet another symmetry, i.e.,

$$W_{pp}^{(\mathrm{sca})}(\theta,\psi_0+90^\circ+\Delta\phi) = W_{pp}^{(\mathrm{sca})}(\theta,\psi_0+90^\circ-\Delta\phi), \tag{35}$$

$$W_{pq}^{(\mathrm{sca})}(\theta,\psi_0+90^\circ+\Delta\phi) = -W_{pq}^{(\mathrm{sca})}(\theta,\psi_0+90^\circ-\Delta\phi) \quad p\neq q. \tag{36}$$

When $B_{xy} \in \mathbb{R}$ and the three coherence radii are equal, the mirror symmetries with respect to the lines ψ_0 and ψ_0+90° of the far-zone quantities can be summarized as:

$$\begin{aligned} &\mathcal{P}^{(\mathrm{sca})}, S_0, \text{ and } S_1 \text{ are even,} \\ &S_2 \text{ and } S_3 \text{ are odd} \end{aligned}$$

The behavior of S_1 and S_2 is illustrated in Fig. 7. Their (anti-)symmetry with respect to the direction ψ_0 (dashed curve) is clearly visible. Both normalized parameters are seen to range approximately from -1 to 1. In both panels the scattering directions that are not shown are copies of the ones that are shown.

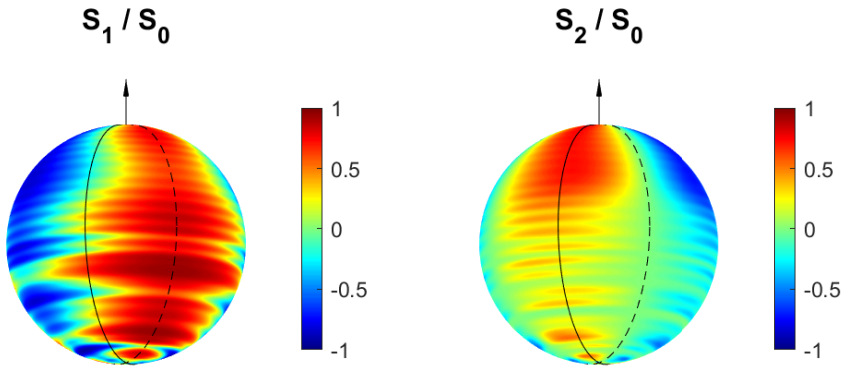

Fig. 7. The normalized Stokes parameter S_1/S_0 (left) and S_2/S_0 (right). These parameters are symmetric and anti-symmetric, respectively, with respect to the polarization direction of the incident field (dashed curve). In this example $B_{xy} = 0.75$ and $\delta_{xx} = \delta_{yy} = \delta_{xy} = 5\lambda$.

Optics EXPRESS

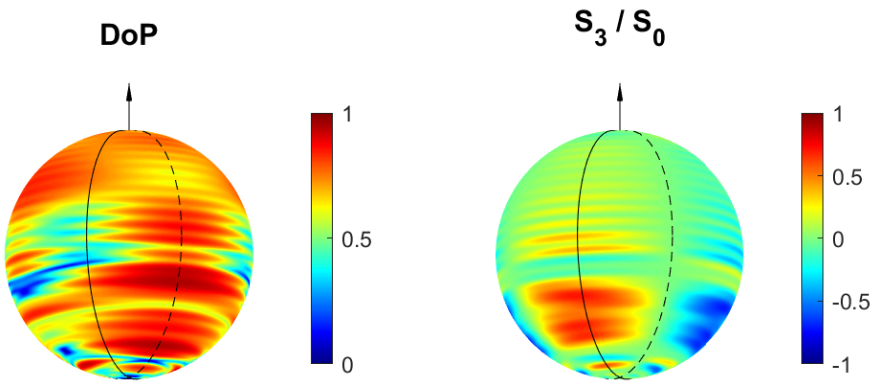

Fig. 8. The degree of polarization of the scattered field (left) and the normalized Stokes parameter S_3/S_0 (right). Notice that the DoP is symmetric with respect to ψ_0 (dashed curve), whereas the Stokes parameter is antisymmetric. The parameters are those of Fig. 7.

In Fig. 8 both the DoP and S_3 are shown. The former is symmetric with respect to ψ_0, whereas the latter is antisymmetric. Note there are directions in which the DoP is quite high, with the polarized portion being essentially circular. In Visualization 2 the full range $0 \le B_{xy} \le 1$ is shown with S_3 normalized by $S_0\,\mathcal{P}^{(\mathrm{sca})}$ to make partial circular polarization visible.

Zeros of the degree of polarization and C-points

When the incident beam is partially linearly polarized, the anti-symmetry of S_2 and S_3 implies they are both zero in the polarization direction, i.e., along the dashed curve in Figs. 7 and 8. Therefore, according to Eq. (28), $\mathcal{P}^{(\mathrm{sca})} = |S_1/S_0|$ there. If in addition S_1 has a zero along this curve, then the scattered field there is completely unpolarized. It turns out that this situation can indeed occur. In the example shown in Fig. 9 the incident field has a DoP $\mathcal{P}^{(\mathrm{inc})} = 0.5$ (blue curve) or 0.75 (red curve). The blue curve's two zero crossings indicate directions in which the scattered is completely unpolarized. If B_{xy} is increased (red curve) these two zeros have been annihilated.

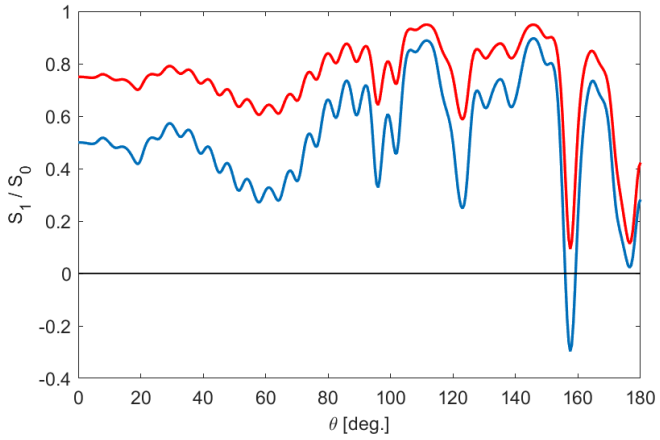

Fig. 9. Normalized Stokes parameter S_1 along the meridian ψ_0 for $B_{xy} = 0.75$ (red) and 0.5 (blue). The two zero crossings of the blue curve near $\theta = 160°$ are directions in which $\mathcal{P}^{(\mathrm{sca})} = 0$. In this example the three radii δ_{ij} are all 5λ.

Optics EXPRESS

The above symmetry arguments hold for a real-valued B_{xy}. If the imaginary part of B_{xy}, which is initially taken to be zero, undergoes a slight perturbation then the two zeros of the DoP disappear. Simultaneously a pair of C-points (points where the polarization ellipse is circular and hence its orientation is singular [20]) is created. In Fig. 10(a), with $\mathrm{Im}\, B_{xy} = 0$, the zeros of all three Stokes parameters coincide. But when the incident field's polarized part becomes slightly elliptical, with $\mathrm{Im}\, B_{xy}>0$, as in Fig. 10(b), the zero contours of S_1 and S_2 intersect in two scattering directions in which the normalized S_3 is plus one. Similarly, when $\mathrm{Im}\, B_{xy}<0$, as in Fig. 10(c), this intersection occurs in directions in which $S_3 = -1$. In the two last cases the polarization singularities have the same handedness as the incident field. Note however that, in the depicted interval, there seems to be a more or less equal set of directions in which the scattered field has a handedness that is opposite from that of the incident beam. The C-points in Fig. 10(b) and (c) occur in regions where $\mathcal{P}^{(\mathrm{sca})}$ is of the order of 1%.

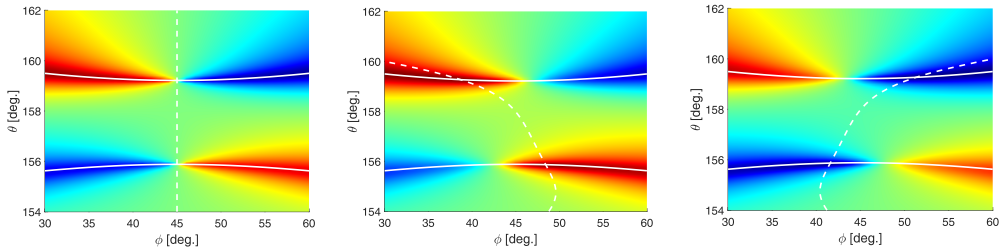

(a) $B_{xy} = 0.5$ (b) $B_{xy} = 0.5 + \mathrm{i}0.05$ (c) $B_{xy} = 0.5 - \mathrm{i}0.05$

Fig. 10. Zero contours of S_1 (solid) and S_2 (dashed) superposed on a density plot of S_3 for various values of B_{xy}. The color coding is that of Fig. 8, and all parameters are as in Fig. 9.

Partial circular polarization

If the three radii δ_{ij} are all equal and B_{xy} is purely imaginary, it follows from Eq. (3) that only S_0 and S_3 are non-zero, meaning that the incident beam is partially circularly polarized. In general, the scattered field will not be partially circularly polarized, rather, all its Stokes parameters will be non-zero. As is to be expected, the scattered field's DoP and its four Stokes parameters are now symmetric about the z-axis. An example of the former is shown in Fig. 11. As before, the DoP of the scattered field can either be much higher or much lower than that of the incident field which in this case has $\mathcal{P}^{(\mathrm{inc})} = 0.6$.

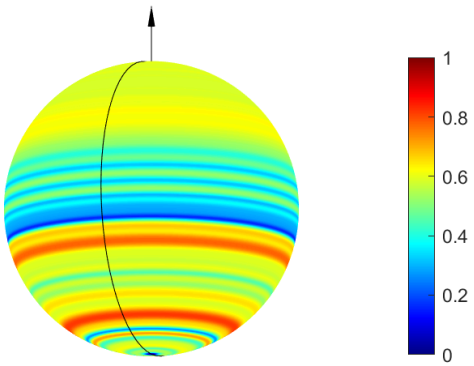

Fig. 11. The degree of polarization of the scattered field for the case that the incident beam is partially circular polarized. In this example the three radii δ_{ij} are all 5λ, and $B_{xy} = \mathrm{i}0.6$, hence $\mathcal{P}^{(\mathrm{inc})} = 0.6$.

Optics EXPRESS

The three coherence radii

The Stokes parameters as well as the DoP of the *incident* beam, as given by Eqs. (3) and (28), are seen to be independent of the coherence radii. However, the polarization state of the *scattered* field does depend on them, as is obvious from Eq. (23). We illustrate this dependence for the DoP with two examples. In Fig. 12(a) the three coherence radii are increased from 5λ (as in Fig. 8), to 10λ, which corresponds to two times the particle radius. Two effects are clearly visible. First, the modulation of the DoP along the θ-direction is now much faster. This is reminiscent of a similar effect found for the spectral density found in scalar studies [6,7]. Second, even though the coherence radii are considerably larger than the particle size, the DoP in many directions is still much lower than $\mathcal{P}^{(\mathrm{inc})} = 0.75$.

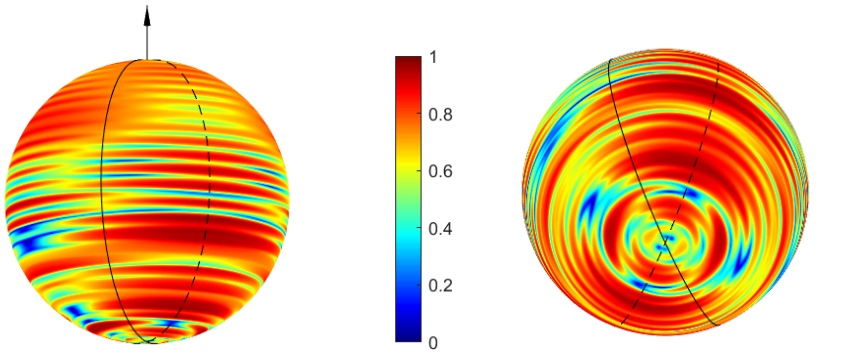

(a) $\delta_{xx} = \delta_{yy} = \delta_{xy} = 10\lambda$

(b) $\delta_{xx} = 5\lambda$, $\delta_{yy} = 10\lambda$, and $\delta_{xy} = 7.91\lambda$

Fig. 12. The far-zone degree of polarization for different values of the coherence radii. Here $\mathcal{P}^{(\mathrm{inc})} = B_{xy} = 0.75$.

The second example is shown in panel (b) of Fig. 12. Now the three coherence radii are unequal ($\delta_{xx} = 5\lambda$, $\delta_{yy} = 10\lambda$, and $\delta_{xy} = 7.91\lambda$). The mirror symmetry with respect to the direction of polarization (dashed curve) is now broken. However, the point symmetry expressed by Eq. (32) remains intact.

As remarked above in connection with Fig. 6, when the incident beam is fully polarized but not fully coherent, the scattered field will not be completely polarized in all directions. Even if all the coherence radii are significantly larger than the sphere, the scattered field in certain directions has a low degree of polarization. This is illustrated in Fig. 13 for the case that all coherence radii are four times larger than the sphere radius. Shown are the spectral density and the DoP along a curve ϕ = constant. Although in general the DoP is quite high, it is still seen to exhibit several deep minima. The inset shows the DoP with the same color coding as in the previous figures. We note that the deep minima of the DoP occur in directions in which the scattered spectral density is appreciable.

Optics EXPRESS

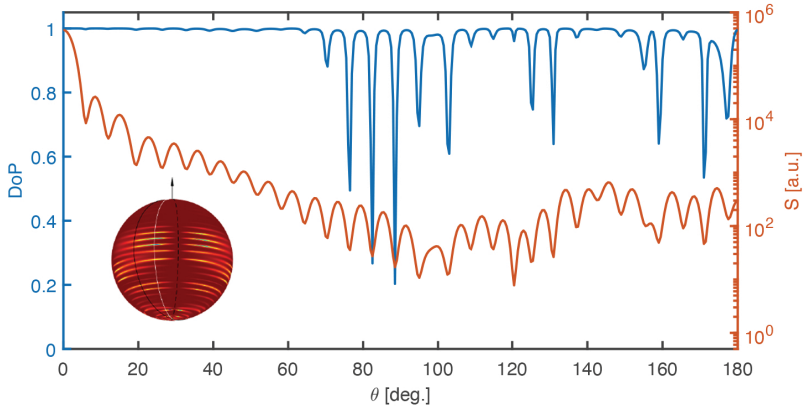

Fig. 13. The degree of polarization $\mathcal{P}^{(\mathrm{sca})}$ (blue) and the spectral density (red) for an incident beam that is fully polarized ($B_{xy} = 1$), and with coherence radii that are four times larger than the sphere radius. Both curves are taken along the meridian $\phi = 22°$. Furthermore, $\delta_{xx} = \delta_{yy} = \delta_{xy} = 20\,\lambda$. Inset: the DoP, with the white curve representing the $\phi = 22°$ meridian.

4. Conclusions

We have studied the effects of spatial coherence and polarization of a beam on its scattering by a dielectric sphere. The degree of polarization of the scattered field can either be much larger or much smaller than that of the incident field. Surprisingly, due to partial coherence, a fully polarized beam can generate a scattered field with a low DoP. The presence or absence of symmetry properties of the far-zone scattered field were found to be dependent on the three coherence radii.

The choice of Gaussian-correlated fields is inspired by the fact that such correlations, due to the Central Limit Theorem, are commonly encountered. In earlier work (scalar) Bessel-correlated beams were found to have different scattering properties [8,9,21].

Our results may find application in atmospheric and climate studies, but also in the analysis of light scattering in colloidal suspensions, which was the topic of Gustav Mie's seminal work [22].

Disclosures. The authors declare no conflicts of interest.

Data availability. No data were generated or analyzed in the presented research.

Supplemental document. See Supplement 1 for supporting content.

References

1. L. Mandel and E. Wolf, *Optical Coherence and Quantum Optics* (Cambridge University, 1995).
2. E. Wolf, *Introduction to the Theory of Coherence and Polarization of Light* (Cambridge University, 2007).
3. C.F. Bohren and D.R. Huffman, *Absorption and Scattering of Light by Small Particles* (Wiley and Sons, 1998).
4. W. Hergert and T. Wriedt, *The Mie Theory* (Springer, 2012).
5. J. J. Greffet, M. de la Cruz-Gutierrez, P. V. Ignatovich, *et al.*, "Influence of spatial coherence on scattering by a particle," J. Opt. Soc. Am. A **20**(12), 2315–2320 (2003).
6. T. van Dijk, D. G. Fischer, T. D. Visser, *et al.*, "Effects of spatial coherence on the angular distribution of radiant intensity generated by scattering on a sphere," Phys. Rev. Lett. **104**(17), 173902 (2010).
7. D. G. Fischer, T. van Dijk, T. D. Visser, *et al.*, "Coherence effects in Mie scattering," J. Opt. Soc. Am. A **29**(1), 78–84 (2012).
8. Y. Wang, H. F. Schouten, and T. D. Visser, "Tunable, anomalous Mie scattering using spatial coherence," Opt. Lett. **40**(20), 4779–4782 (2015).
9. Y. Wang, H. F. Schouten, and T. D. Visser, "Strong suppression of forward or backward Mie scattering by using spatial coherence," J. Opt. Soc. Am. A **33**(4), 513–518 (2016).
10. H. F. Schouten, D. G. Fischer, and T. D. Visser, "Coherence modification and phase singularities on scattering by a sphere: Mie formulation," J. Opt. Soc. Am. A **36**(12), 2005–2010 (2019).

Optics EXPRESS

11. S. A. Wadood, H. F. Schouten, D. G. Fischer, *et al.*, "Anomalous spatial coherence changes in radiation and scattering," Opt. Express **29**(14), 21300–21312 (2021).
12. D. Cabaret, S. Rossano, and C. Brouder, "Mie scattering of a partially coherent beam," Opt. Commun. **150**(1-6), 239–250 (1998).
13. J. Liu, L. Bi, P. Yang, *et al.*, "Scattering of partially coherent electromagnetic beams by water droplets and ice crystals," J. Quant. Spectrosc. Radiat. Transfer **134**, 74–84 (2014).
14. M. Lahiri and E. Wolf, "Theory of refraction and reflection with partially coherent electromagnetic beams," Phys. Rev. A **86**(4), 043815 (2012).
15. M. Lahiri and E. Wolf, "Change in spatial coherence of light on refraction and on reflection," J. Opt. Soc. Am. A **30**(6), 1107–1112 (2013).
16. S. Divitt and L. Novotny, "Spatial coherence of sunlight and its implications for light management in photovoltaics," Optica **2**(2), 95–103 (2015).
17. R. Carminati and J. C. Schotland, *Principles of Scattering and Transport of Light* (Cambridge University Press, 2021).
18. F. Gori, M. Santarsiero, R. Borghi, *et al.*, "Realizability condition for electromagnetic Schell-model sources," J. Opt. Soc. Am. A **25**(5), 1016–1021 (2008).
19. M. Born and E. Wolf, *Principles of Optics* (Cambridge University, 1999).
20. G.J. Gbur and E. Wolf, *Singular Optics* (CRC Press, 2017).
21. Y. Wang, S. Yan, D. Kuebel, *et al.*, "Dynamic control of light scattering using spatial coherence," Phys. Rev. A **92**(1), 013806 (2015).
22. G. Mie, "Beiträge zur Optik trüber Medien, speziell kolloidaler Metallösungen," Ann. Phys. (Berlin, Ger.) **330**(3), 377–445 (1908).